Research Article **Open Access**

Long Nguyen, Maziar Raissi, and Padmanabhan Seshaiyer*

Modeling, Analysis and Physics Informed Neural Network approaches for studying the dynamics of COVID-19 involving human-human and human-pathogen interaction

https://doi.org/10.1515/cmb-2022-0001
Received September 2, 2021; accepted January 10, 2022

Abstract: In this work, the dynamics of the spread of COVID-19 is considered in the presence of both human-to-human transmission as well as environment-to-human transmission. Specifically, we expand and modify traditional epidemiological model for COVID-19 by incorporating a compartment to study the dynamics of pathogen concentration in the environmental reservoir, for instance concentration of droplets in closed spaces. We perform a mathematical analysis for the model proposed including an endemic equilibrium analysis as well as a next-generation approach both of which help to derive the basic reproduction number. We also study the efficacy of wearing a facemask through this model. Another important contribution of this work is the introduction to physics informed deep learning methods (PINNs) to study the dynamics. We propose this as an alternative to traditional numerical methods for solving system of differential equations used to describe dynamics of infectious diseases. Our results show that the proposed PINNs approach is a reliable candidate for both solving such systems and for helping identify important parameters that control the disease dynamics.

Keywords: COVID-19 Model, Compartmental Models, Deep Learning

MSC: 92-08, 92-10, 92BXX, 34AXX, 68T07

1 Introduction

COVID-19 caused by a novel coronavirus has continued to pose as a serious public health risk. Despite global efforts to employ several health care strategies for minimizing the impact of the coronavirus on the community, there is still a great need to understand the dynamics of the virus as it transmits from human to human. Mathematical models with computational simulations have been very effective tools that help such global efforts to understand the dynamics of the disease, to estimate key transmission parameters and to make further improvements for controlling this disease.

Most of these models build on modifying the well-known susceptible-exposed-infectious-recovered (SEIR) compartmental mathematical model for prediction of disease epidemic dynamics [4]. An SEIR model was introduced to describe the transmission dynamics, and helped to forecast the national and global spread

Long Nguyen: George Mason University, Fairfax, Virginia, USA
Maziar Raissi: University of Colorado, Boulder USA
***Corresponding Author: Padmanabhan Seshaiyer:** George Mason University, Fairfax, Virginia, USA,
E-mail: pseshaiy@gmu.edu

of COVID-19, based on reported data from December 31, 2019 to January 28, 2020 [30]. A deterministic compartmental model incorporating the clinical progression of the disease, the individual epidemiological status, and intervention measures was later proposed [29]. Some of the latter developments have included studies focusing on effect of interventions [7, 20] social heterogeneity [9, 21], controlled simulation strategies [16], and spatial propagations with diffusion and reaction terms [17]. While most of these studies focused on human-to-human transmission pathways, many of these do not account for the influence of environment in the transmission of COVID-19 [19, 31]. Since environmental samples were believed to have been taken from seafood markets that have come positive for the novel coronavirus [12], it seems to suggest that the pathogen may also be transmitted through the environmental reservoir. There are studies that also suggest the possibility of the virus surviving in such environments for days which brings to the focus of this paper.

In this paper, we consider the dynamics of COVID-19 in enclosed spaces such as an aircraft cabin or a closed room. When infected individuals cough or sneeze, they may spread the virus to the environment through their respiratory droplets which may then go on to infect other people who are in close contact. Along with the human-to-human transmission, one can also consider an environment-to-human transmission by introducing an environmental compartment that represents the pathogen concentration in the environmental reservoir. In this work, we introduce such a modified SEIR model that includes the dynamics of a pathogen denoted by P and hence the SEIRP model. We perform a mathematical analysis of the model deriving an endemic equilibrium that leads to the basic reproduction number which is validated using a next-generation matrix approach as well [8, 10, 22].

Finally, most of the models that have been introduced rely on numerical methods such as the fourth order Runge-Kutta or other powerful methods to solve the coupled system of differential equations that are formulated via a compartmental system describing the disease dynamics. However, these models often assume some known data for the transmission and recovery parameters. One of the grand challenges in mathematical biology and epidemiology is therefore to develop a coherent deep learning framework that enables researchers to blend differential equations with the vast data sets now available to estimate these parameters efficiently. One of these approaches is to use neural networks which is a system of decisions modeled after the human brain. In this work, we also present a new paradigm of learning differential equations from limited data for infectious diseases. In particular, we will introduce hidden physics models for the SEIRP model, which are essentially data-efficient learning machines capable of leveraging on the underlying laws of physics, expressed by time-dependent differential equations, to extract patterns from high-dimensional data generated from experiments and learn the parameters.

The outline of the paper is as follows. In section 2, we introduce the mathematical model along with the system of governing differential equations. In section 3, we conduct a mathematical analysis of the model through an endemic equilibrium approach and a next-generation approach that both yield the basic reproduction number. Section 4 introduces the PINNs deep learning approach for solving infectious diseases through the model presented in this work. In Section 5, we conduct a variety of computational experiments to validate the PINNs method as a forward solver, inverse solver and a solver in the presence of limited datasets. Finally, we discuss and conclude in Section 6.

2 Mathematical Model and Governing Equations

In this work, we introduce a modified SEIR model that describes the disease dynamics through both a human-human interaction as well as a human-pathogen P interaction. The model is organized around the following flow diagram (see Figure 1). Note that the dashed lines refer to human-to-human transmission and dotted lines refer to human-to-pathogen transmission.

The COVID-19 disease transmission dynamics within this model is then given by the following SEIRP governing differential equations:

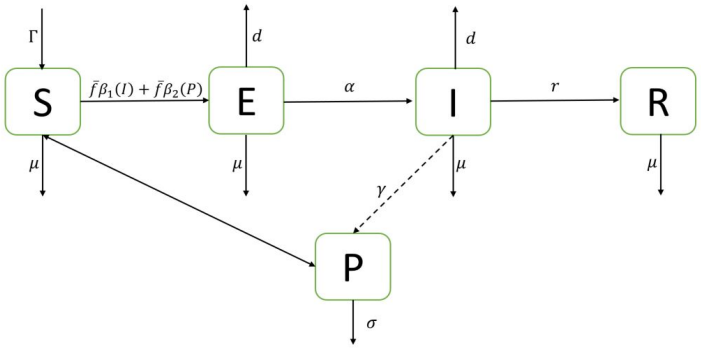

Figure 1: The flow diagram describing the interaction of human-pathogen populations

$$\frac{dS}{dt} = \Gamma - \beta_1(I)\bar{f}SI - \beta_2(P)\bar{f}SP - \mu S \tag{1}$$

$$\frac{dE}{dt} = \beta_1(I)\bar{f}SI + \beta_2(P)\bar{f}SP - \alpha E - dE - \mu E \tag{2}$$

$$\frac{dI}{dt} = \alpha E - rI - dI - \mu I \tag{3}$$

$$\frac{dR}{dt} = rI - \mu R \tag{4}$$

$$\frac{dP}{dt} = \gamma I - \sigma P \tag{5}$$

In a population of $N = S + E + I + R$ humans and P pathogens, the susceptible humans S are assumed to interact with infected individuals as well as the pathogen in the environment and move to the exposed class E after acquiring the disease. The transmission is being modeled via the addition of terms directly proportional to the respective infected human class I involved in the interaction and an infection rate proportional to the pathogen population. The transmission function $\beta_1(I) = \dfrac{\beta_1}{1 + c_1 I}$ represents the direct, human-to-human transmission between the infected and susceptible individuals with β_1 as the rate of transmission from S to E due to contact with I and c_1 as the proportion of interaction with an infectious individual. Similarly, the transmission function $\beta_2(P) = \dfrac{\beta_2}{1 + c_2 P}$ represents the indirect, environment-to-human transmission rate with β_2 as the transmission rate from S to E due to contact with P and c_2 as the proportion of interaction with the pathogens in the environment. Both $\beta_1(I)$ and $\beta_2(P)$ are assumed to be non-increasing functions given that higher values of I and P would motivate stronger control measures that could reduce the transmission rates.

Note that the exposed category models the incubation period before a human becomes infectious. Members of the exposed class E move to become infectious at a human incubation rate of α which is intrinsic human latent period. Members from the infectious classes recover with rate r. Note that we also assume a COVID-19 disease related death rate d for the exposed and infected classes. We assume a population influx represented by Γ and μ to be natural death rate of the various human population states. The pathogen P describing the concentration of the coronavirus in the environment is expected to grow by being exposed to the infected individuals at a rate of γ and also be removed from the system due to a loss of infectivity σ. Finally, $\bar{f} = 1 - f$ where f denotes efficacy of the face mask worn by the susceptible population.

3 Analysis of the Mathematical Model

First, note that the disease free equilibrium (DFE) for the system (1)-(5) is given by:

$$(S_0, E_0, I_0, R_0, P_0) = \left(\frac{\Gamma}{\mu}, 0, 0, 0, 0\right). \tag{6}$$

Next, one can note that all the solutions of the proposed SEIRP model with its initial conditions $\{S_0, E_0, I_0, R_0, P_0\} \geq 0$ are a subset in the interval $[0, \infty)$ for all $0 \leq t < \infty$. For,

$$\Gamma - \beta_1(I)\bar{f}SI - \beta_2(P)\bar{f}SP \geq 0$$

in (1), one can obtain the inequality $\dot{S} \geq -\mu S$ which yields $S(t) \geq S(0)e^{-\mu t} \geq 0$. Hence, $S(t)$ is a non-negative function for all values $t \in [0, \infty)$. In a similar fashion, one can show that $E(t), I(t), R(t), P(t)$ are all also non-negative functions for all values $t \in [0, \infty)$.

Next, we will derive the *basic reproduction number* $\mathcal{R}_0$ for the system system (1) - (5) which denotes the number of secondary infections generated by an infected pathogen or human when the population being considered is composed of primarily susceptible humans and pathogens.

3.1 Endemic equilibrium for the SEIRP model

Setting the derivatives for the system (1) - (5) to be zero yields:

$$0 = \Gamma - \beta_1(I^\star)\bar{f}S^\star I^\star - \beta_2(P^\star)\bar{f}S^\star P^\star - \mu S^\star \tag{7}$$

$$0 = \beta_1(I^\star)\bar{f}S^\star I^\star + \beta_2(P^\star)\bar{f}S^\star P^\star - \alpha E^\star - dE^\star - \mu E^\star \tag{8}$$

$$0 = \alpha E^8 - rI^\star - dI^\star - \mu I^\star \tag{9}$$

$$0 = rI^\star - \mu R^\star \tag{10}$$

$$0 = \gamma I^\star - \sigma P^\star \tag{11}$$

From equation (9) we get:

$$E^\star = \frac{(r + d + \mu)}{\alpha} I^\star \tag{12}$$

Using equations (7) and (11), we get,

$$S^\star = \frac{\Gamma}{\mu + \bar{f}\left(\beta_1(I^\star) + \frac{\gamma}{\sigma}\beta_2(P^\star)\right) I^\star} \tag{13}$$

Substituting equations (11), (12) and (13) in (8) and defining $C = \frac{\sigma\mu}{\bar{f}\left[\sigma\beta_1(I) + \gamma\beta_2(P)\right]} > 0$ we can solve for $I^\star$ using the quadratic equation

$$\left(I^\star\right)^2 - C\left(\frac{\Gamma}{\mu S^\star} - 1\right) I^\star = 0$$

which yields

$$I^\star = C\left(\frac{\Gamma}{\mu S^\star} - 1\right) \tag{14}$$

In equation (14) note that $I^\star > 0$ if $\frac{\Gamma}{\mu S^\star} > 1$. Using equation (13), this ratio that can be simplified to yield the basic reproduction number $\mathcal{R}_0$ given by:

$$\mathcal{R}_0 = \frac{\Gamma}{\mu}\left\{\frac{\alpha\bar{f}\beta_1(I^\star)}{(\alpha + d + \mu)(r + d + \mu)} + \frac{\alpha\bar{f}\gamma\beta_2(P^\star)}{\sigma(\alpha + d + \mu)(r + d + \mu)}\right\} \tag{15}$$

Using (13), (14) and (15), note that we can rewrite, $(S^\star, E^\star, I^\star, R^\star, P^\star)$

$$\left(\frac{\Gamma}{\mu\mathcal{R}_0},\ \frac{(r + d + \mu)}{\alpha} C(\mathcal{R}_0 - 1),\ C(\mathcal{R}_0 - 1),\ \frac{r}{\mu} C(\mathcal{R}_0 - 1),\ \frac{\gamma}{\sigma} C(\mathcal{R}_0 - 1)\right) \tag{16}$$

Note that if $\mathcal{R}_0 = 1$, we recover the disease free equilibrium in equation (6). If $\mathcal{R}_0 > 1$, then the system (1)-(5) has a unique endemic equilibrium $(S^\star, E^\star, I^\star, R^\star, P^\star)$ [18].

3.2 Next Generation Matrix Approach

An alternative method to compute the basic reproduction number $\mathcal{R}_0$ is using the next generation matrix approach [8, 10, 22] which we apply to our SEIRP system (1)-(5).

Theorem 3.1. *The basic reproduction number $\mathcal{R}_0$ is given by:*

$$\mathcal{R}_0 = \mathcal{R}_0^a + \mathcal{R}_0^b$$

where

$$\begin{aligned} \mathcal{R}_0^a &= \frac{\alpha\beta_1(0)\bar{f}S_0}{(\alpha+d+\mu)(r+d+\mu)} \\ \mathcal{R}_0^b &= \frac{\alpha\gamma\beta_2(0)\bar{f}S_0}{\sigma(\alpha+d+\mu)(r+d+\mu)} \end{aligned}$$

Proof. Given the infectious states: E, I, V in system (1) - (5), we can create a vector $\mathcal{F}$ that represents the new infections flowing only into the exposed compartments given by:

$$\mathcal{F} = \left\{\beta_1(0)\bar{f}S_0 I + \beta_2(0)\bar{f}S_0 P, 0, 0\right\}$$

where $\beta_1(I) = \dfrac{\beta_1}{1+c_1 I}$ and $\beta_1(P) = \dfrac{\beta_2}{1+c_2 P}$ Along with $\mathcal{F}$, we also consider $\mathcal{V}$ which denotes the outflow from the infectious compartments in system (1) - (5) which is given by:

$$\mathcal{V} = \{(\alpha+d+\mu)E, -\alpha E + (r+d+\mu)I, -\gamma I + \sigma P\}$$

Next, we compute the Jacobian matrices F and V from $\mathcal{F}$ and $\mathcal{V}$ respectively given by:

$$F = \begin{pmatrix} 0 & \beta_1(0)\bar{f}S_0 & \beta_2(0)\bar{f}S_0 \\ 0 & 0 & 0 \\ 0 & 0 & 0 \end{pmatrix}$$

$$V = \begin{pmatrix} \alpha+d+\mu & 0 & 0 \\ -\alpha & r+d+\mu & 0 \\ 0 & -\gamma & \sigma \end{pmatrix}$$

One can now calculate the next-generation matrix approach [6, 22] to yield:

$$FV^{-1} = \begin{pmatrix} \dfrac{\alpha\beta_1(0)\bar{f}S_0\sigma + \alpha\beta_2(0)\bar{f}S_0\gamma}{\sigma(\alpha+d+\mu)(r+d+\mu)} & \dfrac{\beta_1(0)\bar{f}S_0\sigma + \beta_2(0)\bar{f}S_0\gamma}{\sigma(r+d+\mu)} & \dfrac{\beta_2(0)\bar{f}S_0}{\sigma} \\ 0 & 0 & 0 \\ 0 & 0 & 0 \end{pmatrix}$$

Solving the characteristic equation corresponding to this $\det(FV^{-1} - \lambda I) = 0$ yields the largest eigenvalue to be

$$\lambda = \frac{\alpha\beta_1(0)\bar{f}S_0\sigma + \alpha\beta_2(0)\bar{f}S_0\gamma}{\sigma(\alpha+d+\mu)(r+d+\mu)}$$

which then gives the expression for the basic reproduction number $\mathcal{R}_0$ as:

$$\mathcal{R}_0 = \mathcal{R}_0^a + \mathcal{R}_0^b$$

where

$$\begin{aligned} \mathcal{R}_0^a &= \frac{\alpha\beta_1(0)\bar{f}S_0}{(\alpha+d+\mu)(r+d+\mu)} \\ \mathcal{R}_0^b &= \frac{\alpha\gamma\beta_2(0)\bar{f}S_0}{\sigma(\alpha+d+\mu)(r+d+\mu)} \end{aligned}$$

□

Remark 3.2. $\mathcal{R}_0^a$ measures the contributions from the human-to-human transmission through infected to susceptible and $\mathcal{R}_0^b$ represents the contribution from the environment-to-human transmission. These two transmissions modes collectively make the overall infection risk for the COVID-19 outbreak.

Remark 3.3. Note that the expression obtained for $\mathcal{R}_0$ matches the expression obtained in equation (15) for DFE $(S_0, E_0, I_0, R_0, P_0) = \left(\frac{\Gamma}{\mu}, 0, 0, 0, 0\right)$.

4 A Deep Learning Approach for solving SEIRP

4.1 Physics Informed Neural Network (PINNs)

Physics Informed Neural Network (PINNs) are deep learning based techniques [24, 25, 26] for solving equations describing multi-physics including ordinary and partial differential, integro-differential and fractional order operators. One of the tools that makes these deep learning methods successful is the use of *neural networks* which is a system of decisions modelled after the human brain [15].

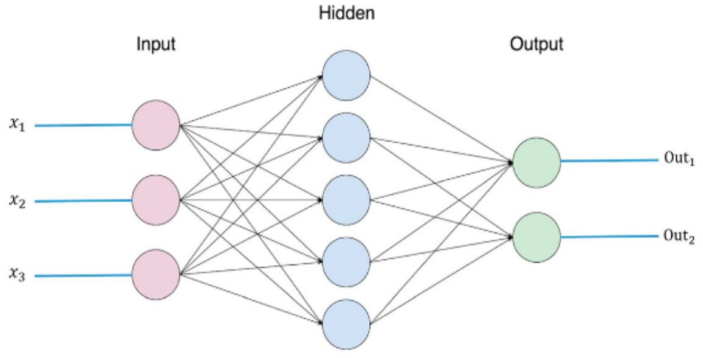

Figure 2: Illustration of a Neural Network

Consider the illustration shown in Figure 2. The first layer of perceptrons first weigh and bias the input which can be observed values of infected data. The next layer then will make more complex decisions based off those inputs, until the final decision layer is reached which generates the outputs which can correspond to the values of parameters in the mathematical model, for instance the transmission and recovery rates. In this work, we implement a physics informed neural network-based approach (PINNs) which makes decisions based on appropriate activation functions depending on the computed *bias* (b) and *weights* (w). The network then seeks to minimize the mean squared error of the regression with respect to the weights and biases by utilizing gradient descent type methods used in conjunction with software such as tensorflow.

Next, we will describe how one can apply such physics informed neural network-based deep learning approaches to the SEIRP system (1)-(5).

4.2 PINNs for SEIRP Model

In the following, inspired by recent developments in PINNs [25], we propose to leverage the hidden physics of infectious diseases (i.e. system (1)-(5)) and infer the latent quantities of interest (i.e. S, E, I, R and P) by approximating them using deep neural networks. This choice is motivated by modern techniques for solving forward and inverse problems associated with differential equations, where the unknown solution is approximated either by a neural network or a Gaussian process. Following these approaches, we approximate the

latent function $t \mapsto (S, E, I, R, P)$ by a deep neural network and obtain the following *physics informed neural networks* (see Figure 3 corresponding to system(1)-(5), i.e.

$$E_1 := \frac{dS}{dt} - \Gamma + \beta_1(I)\bar{f}SI + \beta_2(P)\bar{f}SP + \mu S \tag{17}$$

$$E_2 := \frac{dE}{dt} - \beta_1(I)\bar{f}SI - \beta_2(P)\bar{f}SP + \alpha E + dE + \mu E \tag{18}$$

$$E_3 := \frac{dI}{dt} - \alpha E + rI + dI + \mu I \tag{19}$$

$$E_4 := \frac{dR}{dt} - rI + \mu R \tag{20}$$

$$E_5 := \frac{dP}{dt} - \gamma I + \sigma P \tag{21}$$

A schematic representation of the resulting PINNs for SEIRP is given in Figure 3.

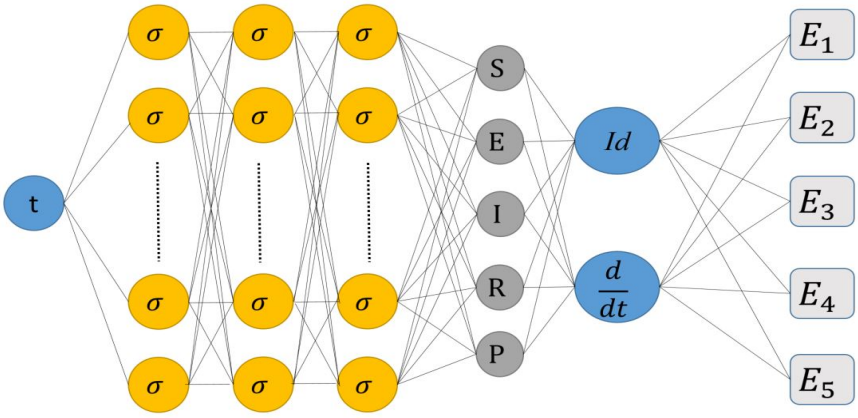

Figure 3: Illustration of the Physics Informed Neural Network Approach [26, 28]

Note that for simplicity of illustration, Figure 3 depicts a network that comprises of three hidden layers and several neurons per hidden layer. Networks with this kind of many-layer structure (with two or more hidden layers) are called *deep neural networks*. These neurons in the network may be thought of as holding numbers that are calculated by a special *activation function* that depends on suitable *weights* and *biases* corresponding to each connection between neurons in each layer. With prior knowledge of such an activation function, the problems boils down to identifying the weights and biases that correspond to computed values of infected data that is close to the observed values. The five sub-populations are approximated by on the deep neural network with calculus on computation graphs using a backpropagation algorithm [11, 13, 27].

We acquire the required derivatives to compute the residual networks E_1, E_2, E_3,E_4 and E_5 by applying the chain rule for differentiating compositions of functions using automatic differentiation [3]. In our formal computations, we employed a densely connected (physics uninformed) neural network, with 3 hidden layers and 90 neurons per hidden layer which takes the input variable t and outputs S, E, I, R, and P. The activation function we employed was $\sigma(x) = \tanh(x)$. We employ automatic differentiation to obtain the required derivatives to compute the residual (physics informed) networks E_1, E_2, E_3, E_4 and E_5. It is worth highlighting that parameters $\{\Gamma, \mu, \alpha, d, r, \gamma, \sigma, \beta_1, \beta_2, c_1, c_2\}$ of the differential equations turn into parameters of the resulting physics informed neural networks $E_1 - E_5$. The total loss function is composed of the regression loss corresponding to the states, $\{S, E, I, R, P\}$ and the loss imposed by the differential equations system (17) - (21). Here, Id denotes the identity operator and the differential operator $\frac{d}{dt}$ is computed using automatic differentiation and can be thought of as an “activation operator". Moreover, the gradients of the loss function

are back-propogated through the entire network to train the parameters using a gradient-based optimization algorithm.

Specifically, we assume that the observables

$$u^M = \{S^n, E^n, I^n, R^n, P^n\}_{n=1}^M$$

are noisy data of size M, that corresponds to the real-world data. Given such data, we are interested in inferring the latent (hidden) quantities $S(t)$, $E(t)$, $I(t)$, $R(t)$ and $P(t)$. The shared parameters of the neural networks for S, E, I, R and P in addition to parameters $\{\Gamma, \mu, \alpha, d, r, \gamma, \sigma, \beta_1, \beta_2, c_1, c_2\}$ of the differential equation system (1)-(5) can be learned by minimizing the sum of squared errors loss function given by,

$$\texttt{Loss} \quad = \quad \frac{1}{N_u}\sum_{j=1}^{N_u}\left(u^j - u^j_{pred}\right)^2 + \frac{1}{N_f}\sum_{k=1}^{N_f}\sum_{i=1}^{5}(E_i^k)^2$$

Here, the first term corresponds to the training data (t^j, u^j) for $j = 1 \ldots N_u$ while the second term enforces the structure imposed by the system (1)-(5) at a finite set of measurement points whose number and locations are taken to be the same as the training data. It should be pointed out that the number and locations of the points on which we enforce the set of differential equations could be different from the actual training data. This procedure is described next by a PINNs algorithm.

4.3 PINNs Algorithm

For a ODE to have a constrained solution space, its temporal domain needs to be constrained. Let us consider a complete ODE problem of the following general form

$$u_t + \mathcal{L}[u;\lambda] \quad = \quad 0, \quad t \in [0, T] \tag{22}$$

$$u(0) \quad = \quad g \tag{23}$$

where $u(t) = \{S(t), E(t), I(t), R(t), P(t)\}$ is the latent solution, $\mathcal{L}[.;\lambda]$ is a nonlinear differential operator parametrized by $\lambda = \{\Gamma, \mu, \alpha, d, r, \gamma, \sigma, \beta_1, \beta_2, c_1, c_2\}$.

There are two types of problems including a forward PINNs problem and an inverse PINNs problems.

- **Forward PINNs**: *Given fixed model parameters λ, find latent solution $u(t)$ at any time t*. Specifically λ is fixed so we minimize **Loss** to obtain weights and biases of the Neural Network to solve for the hidden solutions.
- **Inverse PINNs**: *Given a random data set of data for $u^\star$, we estimate the parameters λ that correspond to the dataset*. Specifically, λ is unknown so we minimize **Loss** to obtain weights, biases of Neural Network and λ as well (estimating parameters). See footnote in the algorithm next.

Algorithm 1: PINNs Forward Algorithm

Result: Give data and the $u_t = -\mathcal{L}[u;\lambda]$ model with initial condition $\mathcal{I}(u) = G$

1ı Initialize to create Neural Networks $\mathcal{N}(t)$ for $t \in \Omega$

2 Input the training Data (t^j, u^j), $j = 1..N_u$

3 Predict the solution u^j_{pred}, $j = 1..N_u$ using the Neural Network $\mathcal{N}(t^j)$

4 Input the data for physics informed (x^k), $k = 1..N_f$

5 Define the residuals $E^k = u_t(t^k) + \mathcal{L}(u(t^k), \lambda)$ for $k = 1..N_f$

6 **while** $n \leq$ `maxiter` **do**

- Define the loss functions `Loss` as follows:

$$\texttt{Loss} \quad = \quad \frac{1}{N_u}\sum_{j=1}^{N_u}\left(u^j - u^j_{pred}\right)^2 + \frac{1}{N_f}\sum_{i=1}^{5}\sum_{k=1}^{N_f}(E_i^k)^2$$

- Train the `Loss` function using Adam's method [1]
- Update weights and biases
- **if** `Loss` $\leq$ `Tol` **then**
  STOP;
  end

end

a Note that in the case of Inverse PINNs, one must also initilize λ

5 Computational Experiments

In this section, we consider the application of PINNS to a variety of scenarios. First we simuulate the application of Forward and Inverse PINNS for system (1)-(5). Following that we present PINNS applied to limited data for a real-world example that was reported in the British Medical Journal Lancet on 4 March 1978 about an outbreak of influenza virus in a boys boarding school [2]. For this we apply PINNS to the classical SIR model.

To start our simulation, we consider the dynamics of the system (1)-(5) with various compartments using traditional Runge-Kutta method for a prescribed set of parameters. We choose values of parameters provided in the literature [19]. Choosing the parameters to be: $\Gamma = 0.00018$; $\beta_1 = 0.00414$; $\beta_2 = 0.0115$; $c_1 = 0.1$; $c_2 = 0.1$; $\mu = 4.563 * 10^{-5}$; $d = 0.0018$; $\alpha = 0.09$; $r = 0.0714$; $\gamma = 0.1$; $\sigma = 0.1724$; $d = 0.0018$; $\bar{f} = 1$.

Let time in days ($t \in [0, 90]$) and initial values given by $S_0 = 9300$, $E_0 = 100$, $I_0 = 10$, $R_0 = 0$, $P_0 = 50$. The various sub-populations are illustrated in Figure 4. Note that we will now use this Runge-Kutta output as input dataset for working with the forward and inverse PINNs algorithm later.

To understand the efficacy of using facemasks, we perform a simulation to plot the total exposed and infected populations for varying values of efficacy of facemasks $f = 0, 0.1, \ldots, 1$. The results of the simulation are shown in Figure 5. Clearly as expected higher the efficacy (value of f) which corresponds to more people wearing facemasks would yield less total number of exposed and infected populations and hence controlling the spread.

5.1 Simulating Forward PINNs

For implementing the PINNs algorithm described earlier, we consider 3 hidden layers with 90 neurons each i.e. Neural Network layers = $[1, 90, 90, 90, 5]$. With $N_u = 200$ (200 data points), $N_f = 300$ (by discretizing $t \in [0, 90]$). We initialized the values of parameters as done earlier for generating Figure 4 and the output of the solution was treated as the input dataset to PINNs. The tolerance was chosen to be 0.05 for the Loss

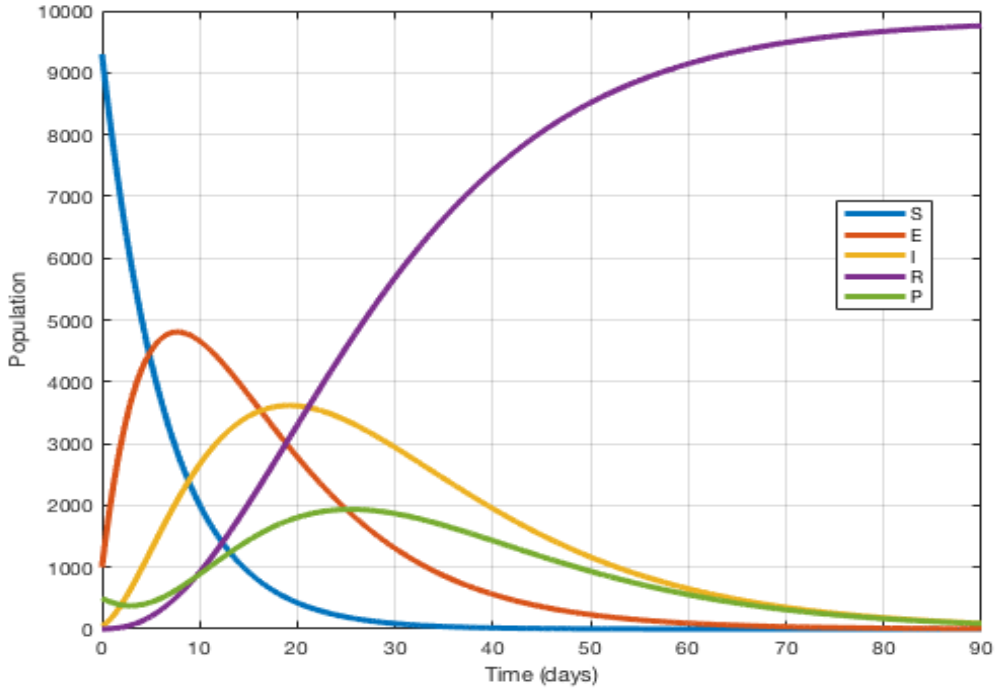

Figure 4: Numerical solution of system (1)-(4) using Runge-Kutta with $\tilde{f} = 1$

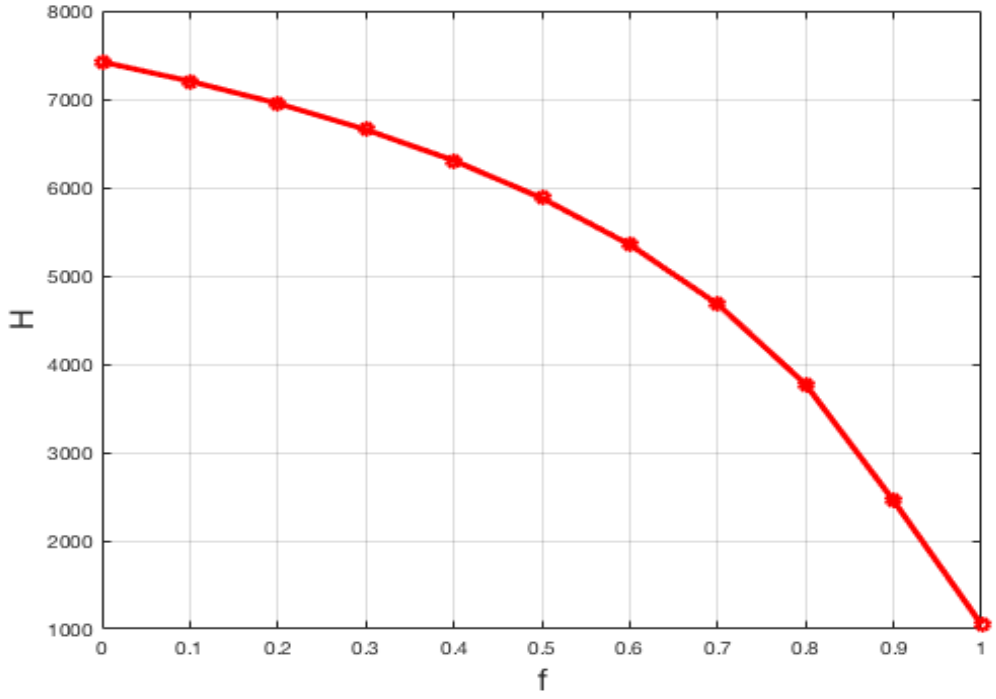

Figure 5: Efficacy of face mask usage in decreasing the number of infected cases

function to satisfy. The results are illustrated in Figure 6. The numerical solution from PINNs validates the numerical data with relative error of 2.9×10^{-3}.

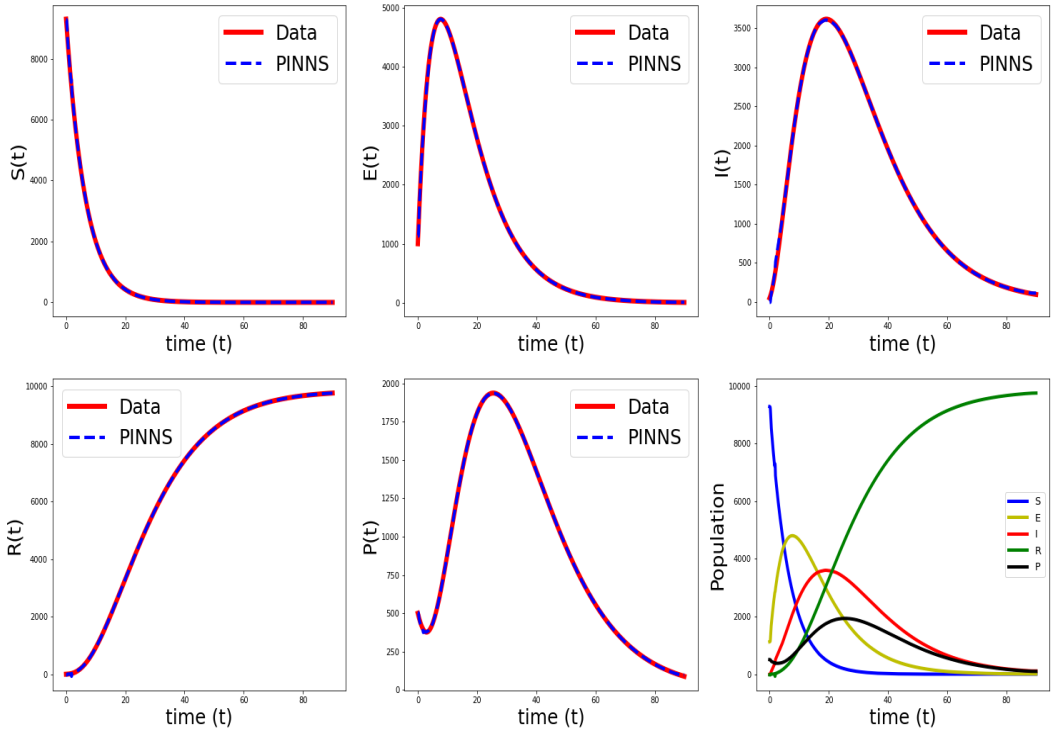

Figure 6: Numerical solution from Forward PINNs validating data

5.2 Simulating Inverse PINNs

We employ the same neural network setup as we used for the Forward PINNs. The only difference is that along with the system state variables, namely, $S(t), E(t), I(t), R(t), P(t)$, we also estimate some of the selected parameters. Here for illustration, we estimate unknown parameters related to the transmission and recovery rates that include $\{\alpha, r, \gamma\}$. In this simulation, we initialize all the unknown parameters to be 1. Given more variables are to be estimated we consider $N_u = 500$ (200 datapoints) and $N_f = 1000$ (by discretizing $t \in [0, 90]$). The tolerance was again chosen to be 0.05 for the Loss function to satisfy.

The results of the parameter estimation by inverse PINNs is illustrated in Figure 7. The estimated value of all the parameters as shown in Figure 7 were computed to be:

$$\alpha = 0.091730, \quad r = 0.072166, \quad \gamma = 0.100041$$

These values are very close to the respective actual values $\alpha = 0.09, r = 0.0714, \gamma = 0.1$ that were used to compute the original numerical data in Figure 4.

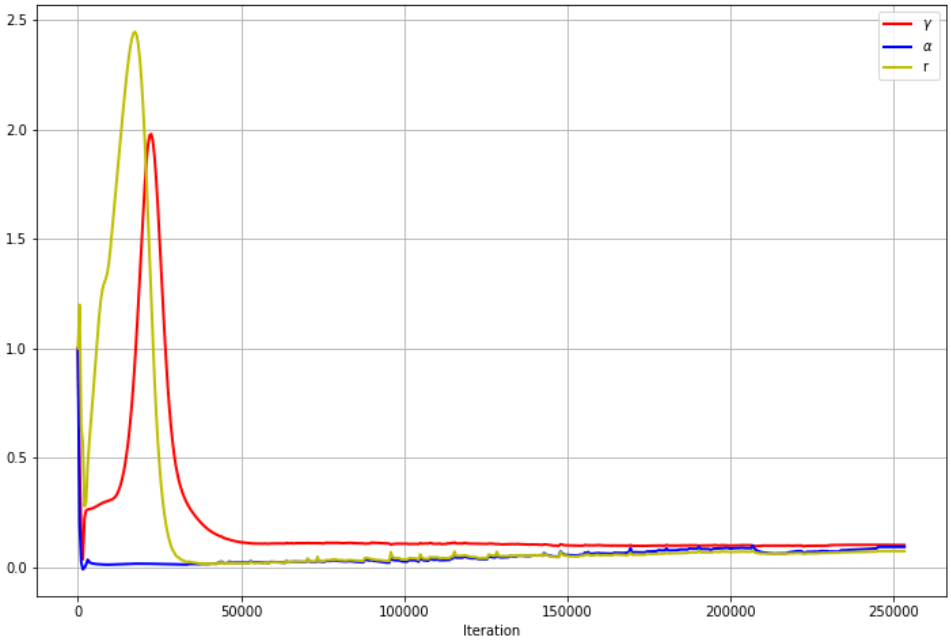

Figure 7: Simulation of Inverse PINNs showing convergence of parameters $\{\alpha, r, \gamma\}$ estimated

5.3 PINNs for Limited Data

There are several advantages of using PINNs over standard numerical approaches that are often used by the infectious diseases community. While fourth order Runge-Kutta methods are preferred for solving governing differential equation systems for infectious disease models, PINNs presents as a good alternative to Runge-Kutta technique with additional features.

First, Physics-informed machine learning integrates seamlessly data and mathematical physics models, even in uncertain and high-dimensional contexts. Next, Kernel-based or neural network-based regression methods offer effective, simple and meshless implementations. Thirdly, estimating parameters for governing differential equations (whether ODEs or PDEs) usually requires lots of data. While there is currently a lot of enthusiasm about 'big data', useful data in infectious diseases is usually 'small' and expensive to acquire. PINNs is very robust with limited data because of adding more physics informed contribution by increasing N_f.

Next, we illustrate this last point by applying PINNs to a well-known limited data set. In 1978, the British Medical Journal Lancet reported on 4 March 1978 about an outbreak of influenza virus in a boys boarding school [2].The school had a population of 763 boys, all of whom were at risk during the epidemic. One boy who had returned from an over sea strip is believed to have initiated an influenza epidemic in the school after his return. There are several papers that have applied a simple epidemic SIR model to study this situation

$$\frac{dS}{dt} = -\beta SI, \tag{24}$$

$$\frac{dI}{dt} = \beta SI - \alpha I, \tag{25}$$

$$\frac{dR}{dt} = \alpha I \tag{26}$$

where S, I and R denoting the susceptible, infected and recovered classes respectively. The susceptible class of individuals included members of the population that have the potential to contract a disease and their size is denoted by S. The infected class of individuals are those that are assumed to have contracted the disease and this class is denoted by I. The final class of individuals denoted by R consisted of those that recovered and cannot contract the disease again. Further, it is also assumed that the number of individuals in each of these classes (compartments) change with time, that is, $S(t)$, $I(t)$ and $R(t)$ are functions of time t and the total population N is the sum of the number of individuals in these compartments. Hence, N = S(t) + I(t) + R(t). So the limited data available include the total population $N = 763$ with a 14 day data with zero recovered cases at the beginning (see Figure 8).

Sample influenza data set (Anonymous,1978)	
Day	Infected number
0	1
1	3
2	8
3	28
4	75
5	221
6	291
7	255
8	235
9	190
10	126
11	70
12	28
13	12
14	5

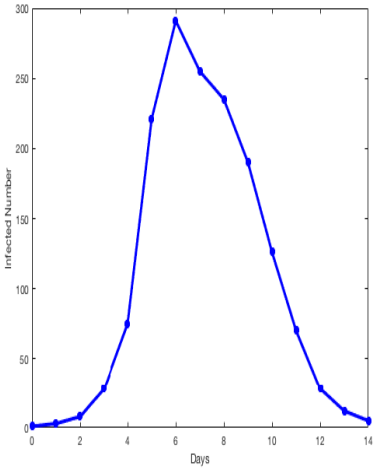

Figure 8: Sample influenza data set (Anonymous,1978)

While there have been multiple studies to estimate α and β, most of them assumed some knowledge about these parameters. We will show that one can use PINNs for estimating α and β with only the limited data information provided and nothing more.

We employed the PINNs approach described earlier to consider 3 hidden layers with 50 neurons each i.e. Neural Network layers = [1, 50, 50, 50, 3]. With $N_u = 15$ (15 data points), $N_f = 800$ (by discretizing $t \in [0, 14]$), we initialized the values of $\alpha_0 = 1$, $\beta_0 = 1$. The $Loss$ function is defined as with $R(0) = 0$,

$$\texttt{Loss} = \frac{1}{N_u}\sum_{j=1}^{N_u}\left(I^j_{train} - I^j_{pred}\right)^2 + \left(R^0_{pred}\right)^2 + \frac{1}{N_f}\sum_{m=1}^{4}\sum_{k=1}^{N_f}(E^k_m)^2$$

Where

$$\begin{aligned} E_1^k &= \frac{dS}{dt} + \beta S^k I^k \\ E_2^k &= \frac{dI}{dt} - \beta S^k I^k + \alpha I^k \\ E_3^k &= \frac{dR}{dt} - \alpha I^k \\ E_1^k &= N - (S^k + I^k + R^k) \end{aligned}$$

Due to the noise in the data, the stopping criteria is defined with a prescribed tolerance $TOL = 0.005$.

$$Stop = |Loss_{iter+1} - Loss_{iter}| \leq TOL$$

Figure 9 illustrates the convergence of the PINNs algorithm to predict the parameters very close to the reported values in the literature $\alpha = 0.45306504, \beta = 0.0022774749$. Figure 10 illustrates how PINNs is more accurate at tracking the dataset in comparison to fourth-order Runge-Kutta. Finally, the power of PINNs is illustrated in Figure 11 which predicts the graph of the latent variables $S(t)$ and $R(t)$ corresponding to the $I(t)$ only knowing that $R(0) = 0$.

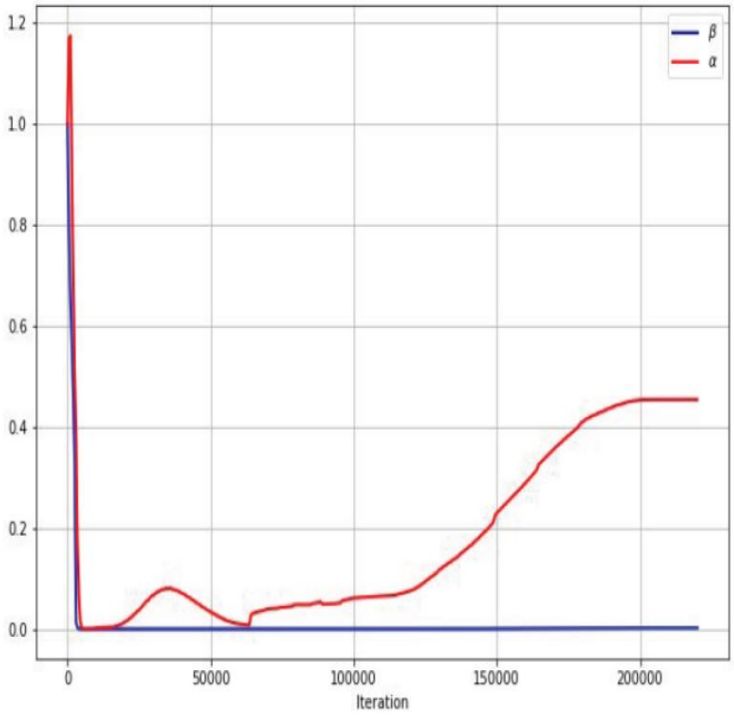

Figure 9: Convergence of the estimated values of parameters α and β

6 Discussion and Conclusion

In this paper the dynamics of COVID-19 in the presence of both human-to-human transmission as well as environment-to-human transmission was considered. The latter was modeled by introducing a compartment that represents the pathogen concentration in the environmental reservoir, for instance concentration of

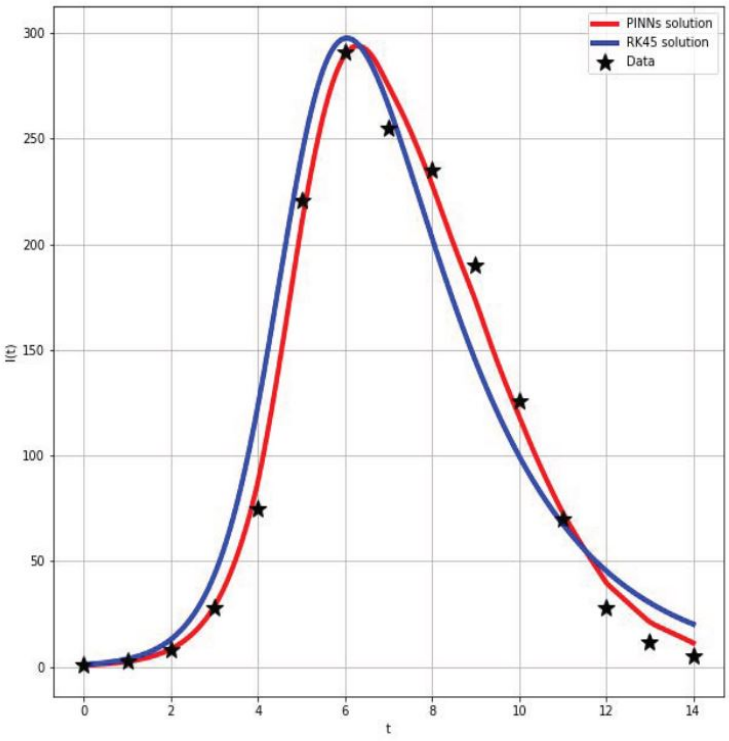

Figure 10: Approximation of the data by PINNs vs. Runge Kutta for the estimated α and β

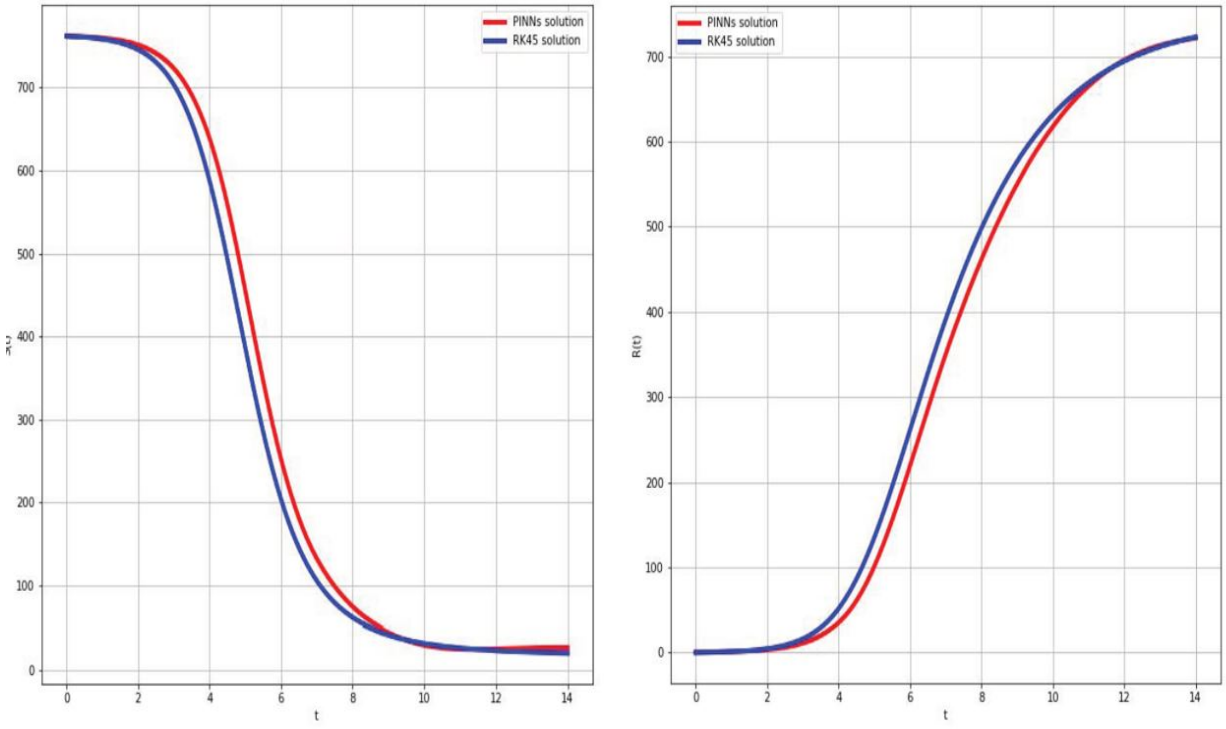

Figure 11: Approximation by PINNs vs. Runge Kutta of $S(t)$ and $R(t)$ corresponding to the $I(t)$ predicted

droplets in closed spaces. The specific compartmental model developed is a SEIRP model that is a modified version of the traditional SEIR compartmental model. We perform a mathematical analysis of the model including an endemic equilibrium analysis as well as a next-generation approach both of which help to derive the basic reproduction number. We also study the impact of wearing a facemask and our results suggest that more people wearing facemasks would help to bring down the number of infected individuals.

Another main contribution of the paper is to introduce the application of physics based deep learning methods for infectious diseases. The method and the algorithm is introduced and applied to the SEIRP model. Because of lack of data, the method was validated with data created using the Runge-Kutta method. Both a forward PINNs for obtaining the solution given a parameter set and an inverse PINNs for obtaining a set of parameters in the model given a solution data set was attempted and successfully solved using PINNs. Finally, we presented other advantages of using deep learning methods such as PINNs when only limited data is present. For this, we considered the famous London boarding school data and validated for an SIR model.

Our results clearly indicate that the models, analysis and computational methods presented are reliable candidates for solving problems involving infectious diseases in epidemiology. The current SEIRP model could be enhanced to include more compartments including dividing the infected individuals to symptomatic and asymptomatic and also including quarantine and hospitalized compartments. This will be considered in a forthcoming paper.

Acknowledgements: This work is supported in part by the National Science Foundation DMS 2031027 and DMS 2031029.

Author's statement

Conflict of interest: Authors state no conflict of interest.

Ethics Statement: This research did not require ethical approval.

References

[1] Kingma, D. P., and Ba, J. (2014). Adam: A method for stochastic optimization. arXiv preprint arXiv:1412.6980.

[2] Anonymous (1978). Influenze in a boarding school. *British Medical Journal*, 1, 578. Retreived from https://www.ncbi.nlm.nih.gov/pmc/articles/PMC1603269/pdf/brmedj00115-0064.pdf

[3] Baydin, A. G., Pearlmutter, B. A., Radul, A. A., and Siskind, J. M. (2018). Automatic differentiation in machine learning: a survey. Journal of Marchine Learning Research, 18, 1-43.

[4] Brauer, F. & Castillo-Chavez, C. (2001). *Mathematical models in population biology and epidemiology* (Vol. 40, pp. xxiv+-416). New York: Springer.

[5] CDC. (2020a). Interim Clinical Guidance for Management of Patients with Confirmed Coronavirus Disease (COVID-19). Retrieved August 6, 2020, from Centers for Disease Control and Prevention website: https://www.cdc.gov/coronavirus/2019-ncov/hcp/clinical-guidance-management-patients.html

[6] Chowell, G., Diaz-Duenas, P., Miller, J. C., Alcazar-Velazco, A., Hyman, J. M., Fenimore, P. W., & Castillo-Chavez, C. (2007). Estimation of the reproduction number of dengue fever from spatial epidemic data. *Mathematical biosciences*, 208(2), 571-589.

[7] Das, A., Dhar, A., Goyal, S., Kundu, A., & Pandey, S. (2021). COVID-19: Analytic results for a modified SEIR model and comparison of different intervention strategies. *Chaos, Solitons & Fractals* 144: 110595.

[8] Diekmann O., Heesterbeek J.A.P. and Metz J.A.J. On the definition and the computation of the basic reproduction ratio R0 in models for infectious diseases in heterogeneous populations. *Journal of Mathematical Biology*, 1990;28(4):365–382.

[9] Dolbeault, J., & Turinici, G. (2021). Social heterogeneity and the COVID-19 lockdown in a multi-group SEIR model. *Computational and Mathematical Biophysics*, *9*(1), 14-21.

[10] van den Driessche P. and Watmough J. Reproduction numbers and sub-threshold endemic equilibria for compartmental models of disease transmission. *Mathematical Biosciences*, 2002;180:29–48.

[11] Goodfellow, I., Bengio, Y., Courville, A., and Bengio, Y. (2016). *Deep learning* (Vol. 1). Cambridge: MIT press.

[12] Gralinski, L. E., & Menachery, V. D. (2020). Return of the Coronavirus: 2019-nCoV. *Viruses*, 12(2), 135.

[13] Hecht-Nielsen, R. (1992). Theory of the backpropagation neural network. In *Neural networks for perception* (pp. 65-93).

[14] Kingma, D. P., and Ba, J. (2014). Adam: A method for stochastic optimization. *arXiv preprint arXiv:1412.6980*.
[15] LeCun, Y., Bengio, Y., and Hinton, G. (2015). Deep learning. nature, 521(7553), 436-444.
[16] López, L., & Rodo, X. (2021). A modified SEIR model to predict the COVID-19 outbreak in Spain and Italy: simulating control scenarios and multi-scale epidemics. *Results in Physics*, 21, 103746.
[17] Mammeri, Y. (2020). A reaction-diffusion system to better comprehend the unlockdown: Application of SEIR-type model with diffusion to the spatial spread of COVID-19 in France. *Computational and Mathematical Biophysics*, 8(1), 102-113.
[18] Martcheva, M. (2015). An introduction to mathematical epidemiology (Vol. 61). New York: Springer.
[19] Mwalili, S., Kimathi, M., Ojiambo, V., Gathungu, D., & Mbogo, R. (2020). EIR model for COVID-19 dynamics incorporating the environment and social distancing, *BMC Research Notes*, 13(1), 1-5.
[20] Ohajunwa, C., Kumar, K., & Seshaiyer, P. (2020). Mathematical modeling, analysis, and simulation of the COVID-19 pandemic with explicit and implicit behavioral changes. *Computational and Mathematical Biophysics*, 8(1), 216-232.
[21] Ohajunwa, C., & Seshaiyer, P. (2021). Mathematical Modeling, Analysis, and Simulation of the COVID-19 Pandemic with Behavioral Patterns and Group Mixing. *Spora: A Journal of Biomathematics*, 7(1), 46-60.
[22] Padmanabhan, P., Seshaiyer, P., & Castillo-Chavez, C. (2017). Mathematical modeling, analysis and simulation of the spread of Zika with influence of sexual transmission and preventive measures. *Letters in Biomathematics*, 4(1), 148-166.
[23] Raissi, M., and Seshaiyer, P. (2014). A multi-fidelity stochastic collocation method for parabolic partial differential equations with random input data. International Journal for Uncertainty Quantification, 4(3).
[24] Raissi, M., and Seshaiyer, P. (2018). Application of local improvements to reduced-order models to sampling methods for nonlinear PDEs with noise. International Journal of Computer Mathematics, 95(5), 870-880.
[25] Raissi, M., and Karniadakis, G. E. (2018). Hidden physics models: Machine learning of nonlinear partial differential equations. Journal of Computational Physics, 357, 125-141.
[26] Raissi, M., Perdikaris, P., and Karniadakis, G. E. (2019). Physics-informed neural networks: A deep learning framework for solving forward and inverse problems involving nonlinear partial differential equations. Journal of Computational Physics, 378, 686-707.
[27] Schmidhuber, J. (2015). Deep learning in neural networks: An overview. *Neural networks*, 61, 85-117.
[28] Shin, Y., Darbon, J., and Karniadakis, G. E. (2020). On the convergence of physics informed neural networks for linear second-order elliptic and parabolic type PDEs. arXiv preprint arXiv:2004.01806.
[29] Tang, B., Wang, X., Li, Q., Bragazzi, N. L., Tang, S., Xiao, Y., & Wu, J. (2020). Estimation of the transmission risk of the 2019-nCoV and its implication for public health interventions. *Journal of clinical medicine*, 9(2), 462.
[30] Wu, J. T., Leung, K., & Leung, G. M. (2020). Nowcasting and forecasting the potential domestic and international spread of the 2019-nCoV outbreak originating in Wuhan, China: a modelling study. *The Lancet*, 395(10225), 689-697.
[31] Yang, C., & Wang, J. (2020). A mathematical model for the novel coronavirus epidemic in Wuhan, China. *Mathematical biosciences and engineering: MBE*, 17(3), 2708.